Frontiers of Information Technology & Electronic Engineering
www.jzus.zju.edu.cn; engineering.cae.cn; www.springerlink.com
ISSN 2095-9184 (print); ISSN 2095-9230 (online)
E-mail: jzus@zju.edu.cn

# Forward link outage performance of aeronautical broadband satellite communications*

Huaicong KONG[1], Min LIN[†‡1], Shiwen HE[2,3], Xiaoyu LIU[1], Jian OUYANG[1], Weiping ZHU[1,4]

[1]*College of Telecommunications and Information Engineering, Nanjing University of Posts and Telecommunications, Nanjing 210003, China*

[2]*School of Computer Science and Engineering, Central South University, Changsha 410083, China*

[3]*Purple Mountain Laboratories, Nanjing 210096, China*

[4]*Department of Electrical and Computer Engineering, Concordia University, Montreal, QC H3G 1M8, Canada*

[†]E-mail: linmin@njupt.edu.cn

Received Aug. 31, 2020; Revision accepted Feb. 1, 2021; Crosschecked May 17, 2021

**Abstract:** High-throughput satellites (HTSs) play an important role in future millimeter-wave (mmWave) aeronautical communication to meet high speed and broad bandwidth requirements. This paper investigates the outage performance of an aeronautical broadband satellite communication system's forward link, where the feeder link from the gateway to the HTS uses free-space optical (FSO) transmission and the user link from the HTS to aircraft operates at the mmWave band. In the user link, spot beam technology is exploited at the HTS and a massive antenna array is deployed at the aircraft. We first present a location-based beamforming (BF) scheme to maximize the expected output signal-to-noise ratio (SNR) of the forward link with the amplify-and-forward (AF) protocol, which turns out to be a phased array. Then, by supposing that the FSO feeder link follows Gamma-Gamma fading whereas the mmWave user link experiences shadowed Rician fading, we take the influence of the phase error into account, and derive the closed-form expression of the outage probability (OP) for the considered system. To gain further insight, a simple asymptotic OP expression at a high SNR is provided to show the diversity order and coding gain. Finally, numerical simulations are conducted to confirm the validity of the theoretical analysis and reveal the effects of phase errors on the system outage performance.

**Key words:** Aeronautical broadband satellite network; Free-space optical (FSO) transmission; High throughput mmWave communication; Outage probability; Phase error

https://doi.org/10.1631/FITEE.2000445 **CLC number:** TN92

## 1 Introduction

Recently, satellite communication (SatCom) has received significant attention because it can provide broadband communication services for mobile users all over the world, especially in remote areas and in the air (Lin et al., 2019, 2020a, 2020b; Huang QQ et al., 2020b; Kong et al., 2020). Since the expected 6$^{\text{th}}$ generation (6G) wireless systems promise to support truly worldwide communication anytime and anywhere, it is foreseen that a future space information network that seamlessly integrates satellite networks with terrestrial networks will become

‡ Corresponding author

* Project supported by the Key International Cooperation Research Project (No. 61720106003), the National Natural Science Foundation of China (No. 61801234), the Shanghai Aerospace Science and Technology Innovation Foundation (No. SAST2019-095), the Research Project of Science and Technology on Complex Electronic System Simulation Laboratory (No. DXZT-JC-ZZ-2019-009), NUPTSF (No. NY220111), and the Postgraduate Research and Practice Innovation Program of Jiangsu Province, China (Nos. KYCX19_0950 and KYCX20_0724)

ORCID: Huaicong KONG, https://orcid.org/0000-0001-8299-6259; Min LIN, https://orcid.org/0000-0002-0296-436X

an ambitious vision in 6G communications (Huang XJ et al., 2019). To meet the continuously increasing demand for high-bandwidth multimedia applications like broadband Internet access, airborne communication, and high-definition (HD)/ultra HD video, high-throughput satellites (HTSs) are playing an important role in SatCom (Sacchi et al., 2019).

In next-generation HTS communication systems, to satisfy the increasing demand for higher data rates, a promising scheme is to move the feeder link, i.e., the link between the gateway and the satellite, from radio frequency (RF) Ka- or Q/V-band to optical frequencies. Compared with RF links, free-space optical (FSO) feeder links have many potential and unique advantages such as larger available bandwidth, unlicensed spectrum resources, immunity to interference, and secure and reliable connection (Kaushal and Kaddoum, 2017). In this context, many studies investigating the application of FSO feeder links in SatCom have been conducted in the literature. Among them, Cianca et al. (2018) provided an overview of the main challenges in exploiting hybrid extremely high-frequency (EHF)/FSO links. Mengali et al. (2016) and Lyras et al. (2019) presented a transmit diversity technique for geostationary Earth orbit (GEO) SatCom systems with optical feeder links. In addition, Ahmad et al. (2017) presented a performance analysis for an optical feeder link multi-beam HTS system, where a zero-forcing (ZF) precoder was used to mitigate inter-beam interference. By considering nonlinear high-powered amplifiers at the transparent fixed gain satellite transponder, Zedini et al. (2020) extended the work in Ahmad et al. (2017) and derived the outage probability (OP), the average bit-error rate (BER), and the ergodic capacity of multi-beam HTS systems. Illi et al. (2020) investigated the physical layer security for a multi-beam HTS system with an FSO feeder link. According to the above mentioned works, it is expected that FSO will be a promising candidate for feeder links in next-generation HTS SatCom systems.

Currently, the user link, i.e., the link between the satellite and users, often operates at the Ku- or Ka-band (Kapusuz et al., 2016; Ahmad et al., 2017). However, because frequency spectrum resources are becoming scarce, the bandwidth spaces in millimeter-wave (mmWave) bands will, in the opinion of many researchers, represent "the new broadband frontier" for next-generation HTS systems. From an industrial perspective, several HTS systems operating in the high-frequency band have been demonstrated in recent years, such as ViaSat-3 and Inmarsat-5 Ka-band satellites. On another front, with the rapid development of the civil aviation market, most passengers on aircraft are eager to enjoy broadband Internet services similar to such services on the ground, which pushes the development of aeronautical broadband satellite communication (Chayot et al., 2017; Jacob et al., 2017). Moreover, with the utilization of mmWave for both air-to-air and air-to-ground transmission, an in-depth understanding of aeronautical mmWave systems is necessary to guarantee reliable aeronautical communication links. To this end, to compensate for the large propagation loss at the mmWave band, satellites commonly employ a high-gain spot beam antenna, while aircraft uses phased array antennas because they are very low profile and easy to employ. Consequently, various research has been carried out to analyze phased array communication systems. For example, Rao et al. (2013) investigated the performance of a low-cost phased array for satellite communication on mobile earth stations. Zhang et al. (2019) studied the BER of communication with a phased array. In addition, Winters and Luddy (2019) proposed a novel technique for maximizing the signal-to-noise ratio (SNR) with phased arrays in typical troposcatter communication systems. However, it is worth mentioning that the above-mentioned works (Rao et al., 2013; Winters and Luddy, 2019; Zhang et al., 2019) have not taken into account the effect of the phase error in phased array antennas, which is important in practical systems. These observations motivate the work presented in this paper.

This paper investigates the outage performance of the forward link of an aeronautical broadband satellite communication system. Specifically, the main contributions of this work are summarized as follows:

1. We present an analytical framework for the forward link of an aeronautical communication system, where HTS is used to improve the system capacity. Here, the feeder link from the gateway to the HTS exploits FSO transmission, while the user link from the HTS to the aircraft operates at the mmWave band. Specifically, concerning the user link, spot beam technology is adopted at the HTS,

and a massive antenna array is employed at the aircraft, which provides broadband access for the passengers in the air.

2. We propose a location-based beamforming (BF) scheme to maximize the expected output SNR of the forward link with the amplify-and-forward (AF) protocol, which turns out to be the phased array. Because the aircraft location information is often obtained through navigation systems, our scheme can avoid the complex procedure of estimating the channel state information (CSI). Moreover, different from the previous works (Rao et al., 2013; Winters and Luddy, 2019; Zhang et al., 2019), we consider the phase errors of the phased array antenna at the aircraft, and derive an analytical expression of the output SNR of a practical aeronautical communication system. We also take satellite antenna gain and path loss into account in the user link.

3. By assuming that the FSO feeder link is subjected to Gamma-Gamma fading and that the mmWave user link is characterized by shadowed Rician (SR) fading, we derive a closed-form OP expression of the forward link for the considered system with the AF protocol. The asymptotic OP expression at high SNR is also presented to reveal the achievable diversity order and coding gain of the system. These OP expressions can largely facilitate the study of the effects of phase errors on the forward link.

Notations: Vectors and matrices are represented by bold lowercase and uppercase letters, respectively. $\mathbb{E}[\cdot]$ is the expectation, $\mathbb{C}^{M\times N}$ is the complex space of $M\times N$, $\boldsymbol{I}_N$ is the $N\times N$ identity matrix, $\mathrm{diag}(\cdot)$ is the diagonal matrix, and $\mathbb{N}^+$ is the set of positive integers. $\mathbb{N}\left(\mu,\sigma^2\right)$ and $\mathbb{CN}\left(\mu,\sigma^2\right)$ represent the real- and complex-valued Gaussian distributions with mean $\mu$ and covariance $\sigma^2$, respectively. $\mathrm{j}=\sqrt{-1}$. $(\cdot)^{\mathrm{T}}$ and $(\cdot)^{\mathrm{H}}$ denote the transpose and Hermitian transpose operations, respectively. $|\cdot|$ and $\|\cdot\|$ stand for the absolute value and the Euclidean norm, respectively. $\Gamma(\cdot)$ denotes the Gamma function, $G[\cdot|\cdot]$ Meijer's G-function, $\mathrm{J}_n(\cdot)$ the first-kind Bessel function of order $n$, $\mathrm{K}_n(\cdot)$ the second-kind modified Bessel function of order $n$, ${}_1F_1(a,b,x)$ the confluent hypergeometric function, and $(a)_p=a(a+1)\cdots(a+p-1)$ the Pochhammer symbol.

## 2 System model

As illustrated in Fig. 1, we consider the forward link of an aeronautical broadband satellite communication system, where an HTS with high-gain spot beam is used to provide a significant boost in system capacity. Specifically, the feeder link employs FSO transmission to take advantage of its unlicensed spectrum, free from interference, and high security, which is regarded as a promising technology in future SatCom (Illi et al., 2020; Zedini et al., 2020). In addition, the mmWave band is exploited for the user link to meet the broad bandwidth demands of aeronautical communications.

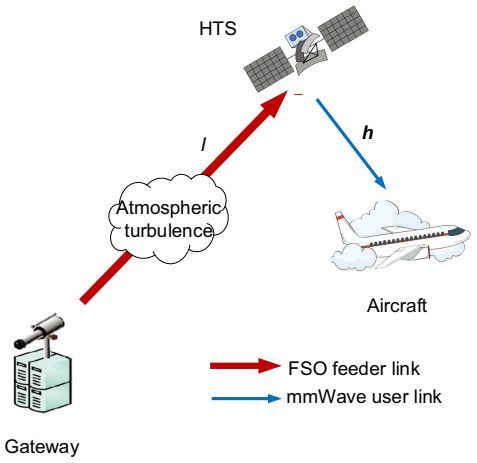


**Fig. 1 System model of the considered network (HTS: high-throughput satellite; FSO: free-space optical)**

The total communication consists of two links. In the FSO feeder link, the gateway sends optical signal $x_1(t)$ satisfying $\mathbb{E}\left[|x_1(t)|^2\right]=1$ to the HTS with transmit power $P_1$. At the HTS, the received optical signal is collected by a telescope and then converted to an electrical signal through a photodetector (Ahmad et al., 2017). As a result, the output electrical signal $y_1(t)$ at the HTS can be expressed as

$$y_1(t)=\sqrt{P_1}\eta I x_1(t)+n_1(t), \tag{1}$$

where $\eta$ is the optical-to-electrical conversion coefficient, $n_1(t)$ is additive white Gaussian noise (AWGN) with zero mean and variance $\sigma_1^2$ (Ahmad et al., 2017), and $I$ is the FSO channel fading coefficient. The channel fading $I$ is assumed to follow a Gamma-Gamma distribution, which is commonly used to model atmospheric turbulence for optical feeder links in SatCom (Illi et al., 2020; Zedini et al.,

2020). Because we consider a limited satellite payload, the AF protocol is often adopted at the HTS. To this end, the received signal $y_1(t)$ is amplified with a variable gain $G=1/\sqrt{P_1\eta^2 I^2+\sigma_1^2}$ and then sent to the aircraft. In the user link, the HTS employs high-gain spot beam technology, while the aircraft is deployed with an antenna array having $N$ elements to compensate for the large propagation loss operating at the mmWave band. Furthermore, by adopting BF technology at the aircraft, the output signal can be denoted as

$$\begin{aligned} y_2(t) =&\boldsymbol{w}^{\mathrm{H}}\left(\sqrt{P_2}G\boldsymbol{h}y_1(t)+\boldsymbol{n}_2(t)\right)\\ =&\sqrt{P_1P_2}G\boldsymbol{w}^{\mathrm{H}}\boldsymbol{h}\eta I x_1(t)+\sqrt{P_2}G\boldsymbol{w}^{\mathrm{H}}\boldsymbol{h}n_1(t)\\ &+\boldsymbol{w}^{\mathrm{H}}\boldsymbol{n}_2(t), \end{aligned} \tag{2}$$

where $P_2$ is the transmit power at the HTS, $\boldsymbol{w}\in\mathbb{C}^N$ the normalized receive BF weight vector at the aircraft, $\boldsymbol{h}\in\mathbb{C}^N$ the channel vector, and $\boldsymbol{n}_2(t)$ the AWGN satisfying $\boldsymbol{n}_2(t)\sim\mathbb{CN}\left(0,\sigma_2^2\right)$. According to Eq. (2), the output SNR at the aircraft can be expressed as

$$\gamma=\frac{\gamma_1\gamma_2}{\gamma_1+\gamma_2+1}, \tag{3}$$

where $\gamma_1=\frac{P_1\eta^2I^2}{\sigma_1^2}\triangleq\bar{\gamma}_1I^2$ with $\bar{\gamma}_1=\frac{P_1\eta^2}{\sigma_1^2}$ and $\gamma_2=\frac{P_2}{\sigma_2^2}\left|\boldsymbol{w}^{\mathrm{H}}\boldsymbol{h}\right|^2\triangleq\bar{\gamma}_2\left|\boldsymbol{w}^{\mathrm{H}}\boldsymbol{h}\right|^2$ with $\bar{\gamma}_2=\frac{P_2}{\sigma_2^2}$.

In what follows, we will discuss the channel models and statistical properties of the output SNRs and thus derive the OP expressions of the considered system.

## 3 Channel models and statistical properties

In this study, because the FSO feeder link is subject to Gamma-Gamma fading, the probability density function (PDF) of channel fading coefficient $I$ in Eq. (1) is given by (Andrews and Phillips, 2005)

$$f_I(I)=\frac{2(\alpha\beta)^{\frac{\alpha+\beta}{2}}}{\Gamma(\alpha)\Gamma(\beta)}I^{\frac{\alpha+\beta}{2}-1}\mathrm{K}_{\alpha-\beta}\left(2\sqrt{\alpha\beta I}\right),I>0, \tag{4}$$

where $\alpha$ and $\beta$ denote the large- and small-scale scintillation parameters related to the atmospheric turbulence conditions, respectively. Furthermore, the PDF expression of $\gamma_1=\bar{\gamma}_1I^2$ in terms of Meijer's G function can be obtained as (Kong et al., 2020)

$$\begin{aligned} f_{\gamma_1}(x)=&\frac{(\alpha\beta)^{\frac{\alpha+\beta}{2}}x^{\frac{\alpha+\beta}{4}-1}}{2\Gamma(\alpha)\Gamma(\beta)\bar{\gamma}_1^{\frac{\alpha+\beta}{4}}}\\ &\cdot G_{0,2}^{2,0}\left[\alpha\beta\sqrt{\frac{x}{\bar{\gamma}_1}}\middle|\begin{matrix}-\\ \frac{\alpha-\beta}{2},-\frac{\alpha-\beta}{2}\end{matrix}\right],x\geq 0. \end{aligned} \tag{5}$$

As for the mmWave channel vector $\boldsymbol{h}\in\mathbb{C}^N$ in Eq. (2), it can be described as $\boldsymbol{h}=\ell\boldsymbol{g}$, in which $\boldsymbol{g}\in\mathbb{C}^N$ represents the channel fading vector and the coefficient $\ell$ is represented as

$$\ell=\frac{c\sqrt{G_{\mathrm{t}}}}{4\pi fd\sqrt{K_{\mathrm{b}}TB}}, \tag{6}$$

where $c$, $f$, and $d$ represent the speed of light, the carrier frequency, and the distance from the HTS to the aircraft, respectively. Meanwhile, $K_{\mathrm{b}}$ denotes the Boltzmann constant, $T$ the noise temperature, and $B$ the noise bandwidth. Also, satellite antenna gain $G_{\mathrm{t}}$ in Eq. (6) can be expressed as (Lin et al., 2019)

$$G_{\mathrm{t}}=G_{\mathrm{t,max}}\left(\frac{\mathrm{J}_1(u_{\mathrm{t}})}{2u_{\mathrm{t}}}+36\frac{\mathrm{J}_3(u_{\mathrm{t}})}{u_{\mathrm{t}}^3}\right), \tag{7}$$

with $G_{\mathrm{t,max}}$ being the maximum satellite transmit antenna gain and $u_{\mathrm{t}}=2.071\,23\sin\theta_{\mathrm{t}}/\sin\theta_{\mathrm{3dB}}$, where $\theta_{\mathrm{t}}$ and $\theta_{\mathrm{3dB}}$ are the angle of pitch between the HTS and the aircraft, and the 3 dB angle of the main beam, respectively. In addition, the channel fading vector $\boldsymbol{g}\in\mathbb{C}^N$ is assumed to follow SR distribution, which is commonly used to describe the satellite link (Abdi et al., 2003; Huang QQ et al., 2020a). In this regard, vector $\boldsymbol{g}$ can be written as

$$\boldsymbol{g}=\bar{\boldsymbol{g}}+\tilde{\boldsymbol{g}}, \tag{8}$$

where $\bar{\boldsymbol{g}}=\rho\boldsymbol{a}(\theta)$ is the line-of-sight (LoS) component with $\rho$ being a random variable (RV) obeying the Nakagami-$m$ distribution with severity parameter $m$ and average power $\Omega$. Suppose that a uniform linear array (ULA) is deployed at the aircraft; thus, the array steering vector $\boldsymbol{a}(\theta)$ is given by

$$\boldsymbol{a}(\theta)=\left[1,\mathrm{e}^{\mathrm{j}\kappa d_{\mathrm{a}}\sin\theta},\cdots,\mathrm{e}^{\mathrm{j}(N-1)\kappa d_{\mathrm{a}}\sin\theta}\right]^{\mathrm{T}}, \tag{9}$$

where $\theta$ is the angle-of-arrival (AoA) of the incoming signal, $\kappa=2\pi/\lambda$ denotes the wavenumber, and $d_{\mathrm{a}}$ denotes the antenna element spacing of the array. In Eq. (8), $\tilde{\boldsymbol{g}}\in\mathbb{C}^N$ denotes the scattering

component which is the independent and identically distributed (i.i.d.) complex Gaussian RV satisfying $\tilde{\boldsymbol{g}} \sim \mathbb{CN}(0, 2b\boldsymbol{I}_N)$ with $2b$ being the average power.

Considering that perfect CSI is often unavailable in an aeronautical communication, we employ a location-based phased array antenna at the aircraft. Therefore, the BF weight vector $\boldsymbol{w}$ can be obtained as given in Lemma 1.

**Lemma 1** The BF weight vector that maximizes the expected output SNR in Eq. (3) is given by

$$\boldsymbol{w}^* = \frac{\boldsymbol{a}(\theta_0)}{\sqrt{N}}. \tag{10}$$

**Proof** See Appendix A.

In practice, although AoA estimation methods can be used to calculate $\theta_0$, they suffer from high implementation complexity. Therefore, in this study, we suppose that the attitude and location information of the aircraft can be obtained through advanced navigation systems, such as the Global Navigation Satellite System (GNSS) (Morales-Ferre et al., 2020). It should be pointed out that navigation is of significant importance for a flying aircraft in the crowed sky of the near future where a great number of drones will coexist with manned aircraft. With the help of Fig. 2, $\theta_0$ can be calculated as

$$\theta_0 = \arctan\left[\frac{\cos\theta_{\mathrm{a}}\cos\varphi_{\mathrm{a}} - 0.151}{\sqrt{1-(\cos\theta_{\mathrm{a}}\cos\varphi_{\mathrm{a}})^2}}\right], \tag{11}$$

where $\theta_{\mathrm{a}}$ and $\varphi_{\mathrm{a}}$ are the latitude of the aircraft in the flat flight condition and the longitude difference between the aircraft and the HTS, respectively. The corresponding proof for the calculation of $\theta_0$ can be found in Appendix B. Using Eq. (10), the output SNR of the user link, i.e., $\gamma_2 = \bar{\gamma}_2\left|\boldsymbol{w}^{\mathrm{H}}\boldsymbol{h}\right|^2$, can be written as

$$\gamma_2 = \bar{\gamma}_2\left(\left|\rho\sqrt{N} + \boldsymbol{v}^{\mathrm{H}}\tilde{\boldsymbol{h}}\right|^2\right). \tag{12}$$

However, due to hardware impairment in practical aeronautical communication, the existing phase error $\varepsilon_n$ should be taken into account, which often satisfies

$$\mathbb{E}[\varepsilon_n] = 0, \tag{13}$$

$$\mathbb{E}\left[\varepsilon_n^2\right] = \sigma^2, \tag{14}$$

$$\mathbb{E}[\varepsilon_m\varepsilon_n] = 0, m \neq n, \tag{15}$$

$$\mathbb{E}\left[\varepsilon_n^k\right] \approx 0, k > 2, \tag{16}$$

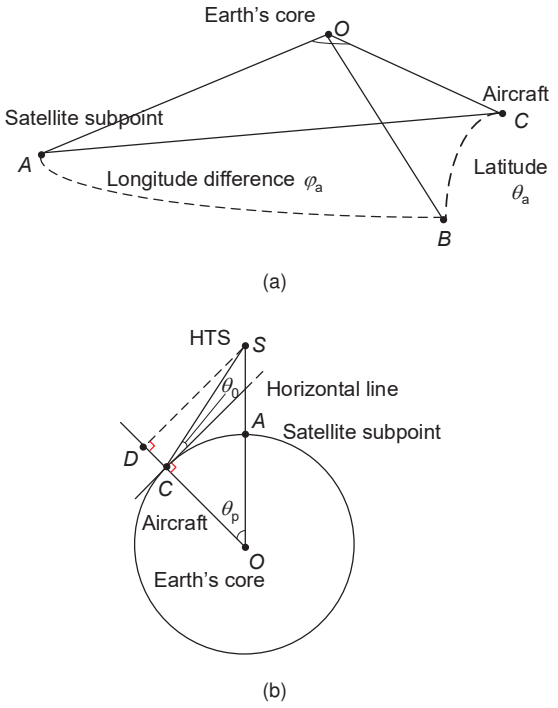


**Fig. 2 Geometrical relation between the HTS and the aircraft: (a) solid figure; (b) plane figure**

$$\mathbb{E}\left[\varepsilon_m^k\varepsilon_n^l\right] \approx 0, k + l > 2. \tag{17}$$

It should be pointed out that in Eq. (14), a larger $\sigma^2$ implies a lower precision of the phase shifter. Moreover, the phase errors of two different phase shifters are assumed to be uncorrelated, i.e., Eq. (15), which is because phase shifting is performed individually by each antenna element. Then, for Eqs. (16) and (17), the moments and mixed moments of order higher than 2 approximately equal zero, because the error is very small and thus its high order is negligible. Based on Eqs. (13)–(17), the output SNR of the user link with phase error present can be obtained as shown in Lemma 2.

**Lemma 2** By taking the phase error into account, the expression for the output SNR of user link $\tilde{\gamma}_2$ is given by

$$\tilde{\gamma}_2 = \bar{\gamma}_2\left(\left|\rho\sqrt{\Phi} + \boldsymbol{v}^{\mathrm{H}}\tilde{\boldsymbol{h}}\right|^2\right), \tag{18}$$

where $\Phi = N + \sigma^2 - N\sigma^2$ with $\sigma^2$ being the variance of phase error RV. Based on Eq. (18), the cumulative

density probability (CDF) of $\tilde{\gamma}_2$ is given by

$$F_{\tilde{\gamma}_2}(x) = 1 - a_1 \sum_{k=0}^{m-1} \frac{(1-m)_k (-a_3)^k}{(a_2-a_3)^{k+1} k!} \exp\left(-\frac{(a_2-a_3)x}{\bar{\gamma}_2}\right) \cdot \sum_{i=0}^{k} \frac{(a_2-a_3)^i}{\bar{\gamma}_2^{n+1} i!} x^i, \tag{19}$$

where $a_2 = \frac{1}{2b}$, $a_1$ and $a_3$ can be, respectively, expressed as

$$a_1 = \frac{1}{2b}\left(\frac{2bm}{2bm+\Phi\Omega}\right)^m, \tag{20}$$

$$a_3 = \frac{\Phi\Omega}{2b(2bm+\Phi\Omega)}. \tag{21}$$

**Proof** See Appendix C.

In the following, we will conduct outage performance analysis for the considered aeronautical broadband satellite communication system.

## 4 Performance analysis

This section will first derive the OP expression of the considered system. Then, asymptotic analysis is carried out to further attain useful insights about the system performance.

### 4.1 Outage probability

The system OP is defined as (Zedini et al., 2020)

$$P_{\text{out}}(\gamma_{\text{th}}) \triangleq \Pr(\tilde{\gamma} \le \gamma_{\text{th}}) = \Pr\left(\frac{\gamma_1 \tilde{\gamma}_2}{\gamma_1 + \tilde{\gamma}_2 + 1}\right). \tag{22}$$

By employing the results given by Trinh and Pham (2015), the system OP in Eq. (22) can be shown as given in Eq. (23) (at the bottom of this page). Then, substituting Eqs. (5) and (19) into Eq. (23), the integration $I_1$ can be expressed as Eq. (24) (at the bottom of this page). With the employment of Eqs. (1.111) and (1.211) in Gradshteyn and Ryzhik (2007), $\left(\gamma_{\text{th}} + \frac{1+\gamma_{\text{th}}}{u-1}\right)^i$ and $\exp\left(-\frac{a_2-a_3}{\bar{\gamma}_2}\frac{1+\gamma_{\text{th}}}{u-1}\right)$ can be, respectively, denoted as

$$\left(\gamma_{\text{th}} + \frac{1+\gamma_{\text{th}}}{u-1}\right)^i = \sum_{j=0}^{i} \binom{i}{j} {\gamma_{\text{th}}}^{i-j} (1+\gamma_{\text{th}})^j (u-1)^{-j}, \tag{25}$$

and

$$\exp\left(-\frac{a_2-a_3}{\bar{\gamma}_2}\frac{1+\gamma_{\text{th}}}{u-1}\right) = \sum_{p=0}^{\infty} \frac{1}{p!(u-1)^p}\left(-\frac{(a_2-a_3)(1+\gamma_{\text{th}})}{\bar{\gamma}_2}\right)^p. \tag{26}$$

Using Eqs. (25) and (26), the integration $I_2$ can be written as Eq. (27) (at the bottom of this page). As

$$P_{\text{out}}(\gamma_{\text{th}}) = 1 - \underbrace{\gamma_{\text{th}} \int_1^{\infty} \left[1 - F_{\tilde{\gamma}_2}\left(\gamma_{\text{th}} + \frac{1+\gamma_{\text{th}}}{u-1}\right)\right] f_{\gamma_1}(u\gamma_{\text{th}}) \mathrm{d}u}_{I_1}. \tag{23}$$

$$I_1 = \frac{a_1 (\alpha\beta)^{\frac{\alpha+\beta}{2}} \gamma_{\text{th}}^{\frac{\alpha+\beta}{4}}}{2\Gamma(\alpha)\Gamma(\beta)\bar{\gamma}_1^{\frac{\alpha+\beta}{4}}} \sum_{k=0}^{m-1} \frac{(1-m)_k (-a_3)^k}{(a_2-a_3)^{k+1} k!} \sum_{i=0}^{k} \frac{(a_2-a_3)^i}{\bar{\gamma}_2^i i!} \exp\left[-\frac{(a_2-a_3)\gamma_{\text{th}}}{\bar{\gamma}_2}\right] \cdot \underbrace{\int_1^{\infty} u^{\frac{\alpha+\beta}{4}-1} \left(\gamma_{\text{th}} + \frac{1+\gamma_{\text{th}}}{u-1}\right)^i \exp\left[-\frac{a_2-a_3}{\bar{\gamma}_2}\frac{1+\gamma_{\text{th}}}{u-1}\right] G_{0,2}^{2,0}\left[\alpha\beta\sqrt{\frac{u\gamma_{\text{th}}}{\bar{\gamma}_1}} \middle| \begin{matrix} - \\ \frac{\alpha-\beta}{2}, -\frac{\alpha-\beta}{2} \end{matrix}\right] \mathrm{d}u}_{I_2}. \tag{24}$$

$$I_2 = \sum_{j=0}^{i} \binom{i}{j} {\gamma_{\text{th}}}^{i-j} (1+\gamma_{\text{th}})^j \sum_{p=0}^{\infty} \frac{1}{p!}\left(-\frac{(a_2-a_3)(1+\gamma_{\text{th}})}{\bar{\gamma}_2}\right)^p \cdot \underbrace{\int_1^{\infty} u^{\frac{\alpha+\beta}{4}-1} (u-1)^{-j-p} G_{0,2}^{2,0}\left[\alpha\beta\sqrt{\frac{u\gamma_{\text{th}}}{\bar{\gamma}_1}} \middle| \begin{matrix} - \\ \frac{\alpha-\beta}{2}, -\frac{\alpha-\beta}{2} \end{matrix}\right] \mathrm{d}u}_{\Theta}. \tag{27}$$

$$P_{\text{out}}(\gamma_{\text{th}}) = 1 - \frac{a_1(\alpha\beta)^{\frac{\alpha+\beta}{2}}\gamma_{\text{th}}^{\frac{\alpha+\beta}{4}}}{2\Gamma(\alpha)\Gamma(\beta)\bar{\gamma}_1^{\frac{\alpha+\beta}{4}}}\sum_{k=0}^{m-1}\sum_{i=0}^{k}\sum_{j=0}^{i}\sum_{p=0}^{\infty}\binom{i}{j}\frac{\gamma_{\text{th}}^{i-j}(1+\gamma_{\text{th}})^j(a_2-a_3)^{i-k-1}(1-m)_k(-a_3)^k}{\bar{\gamma}_2^i i!p!k!} \cdot \exp\left[-\frac{(a_2-a_3)\gamma_{\text{th}}}{\bar{\gamma}_2}\right]\left(-\frac{(a_2-a_3)(1+\gamma_{\text{th}})}{\bar{\gamma}_2}\right)^p \Theta. \tag{32}$$

for the integration $\Theta$ in Eq. (27), we first consider the case of $j+p=0$, namely,

$$\Theta = \int_1^\infty u^{\frac{\alpha+\beta}{4}-1} G_{0,2}^{2,0}\left[\alpha\beta\sqrt{\frac{u\gamma_{\text{th}}}{\bar{\gamma}_1}}\,\middle|\, \begin{matrix} - \\ \frac{\alpha-\beta}{2}, -\frac{\alpha-\beta}{2} \end{matrix}\right] \mathrm{d}u. \tag{28}$$

With the help of Eq. (7.811.3) in Gradshteyn and Ryzhik (2007), $\Theta$ can be expressed as

$$\Theta = 2G_{1,3}^{3,0}\left[\alpha\beta\sqrt{\frac{\gamma_{\text{th}}}{\bar{\gamma}_1}}\,\middle|\, \begin{matrix} 1-\frac{\alpha+\beta}{2} \\ -\frac{\alpha+\beta}{2}, \frac{\alpha-\beta}{2}, -\frac{\alpha-\beta}{2} \end{matrix}\right]. \tag{29}$$

In the case of $j+p>0$, applying the Newton binomial theorem, $(u-1)^{-j-p}\,(j+p>0)$ can be expanded as

$$(u-1)^{-j-p} = \sum_{q=0}^{\infty}\frac{(j+p)_n}{q!}u^{-j-p-q}. \tag{30}$$

By following a similar manner in the first case, $\Theta$ can be expressed as

$$\Theta = 2\sum_{q=0}^{\infty}\frac{(j+p)_n}{q!}G_{1,3}^{3,0}\left[\alpha\beta\sqrt{\frac{\gamma_{\text{th}}}{\bar{\gamma}_1}}\,\middle|\, \begin{matrix} \varpi_2 \\ \varpi_1 \end{matrix}\right], \tag{31}$$

where $\varpi_1 = 2\left(j+p+q-\frac{\alpha+\beta}{4}\right), \frac{\alpha-\beta}{2}, -\frac{\alpha-\beta}{2}$ and $\varpi_2 = 2\left(j+p+q-\frac{\alpha+\beta}{4}\right)+1$.

Finally, the closed-form expression of the system OP can be easily obtained as Eq. (32) (at the top of this page).

**Remark 1** Herein, note that series equations and Meijer's G functions are involved in the OP expression (32). However, the series will converge after using an adequate number of terms, while Meijer's G functions can be calculated easily using mathematical tools such as MATLAB and Mathematica. In the following, a simple asymptotic OP expression will be derived.

### 4.2 Asymptotic analysis

To gain further insights, we now analyze the asymptotic OP for high SNR regions, i.e., $\bar{\gamma}_1, \bar{\gamma}_2 \to \infty$. Similar to the related work (Zedini et al., 2015), the asymptotic OP is given by

$$\begin{aligned} P_{\text{out}}^{\infty}(\gamma_{\text{th}}) &= F_{\gamma_1}^{\infty}(\gamma_{\text{th}}) + F_{\tilde{\gamma}_2}^{\infty}(\gamma_{\text{th}}) - F_{\gamma_1}^{\infty}(\gamma_{\text{th}})F_{\tilde{\gamma}_2}^{\infty}(\gamma_{\text{th}}) \\ &\approx F_{\gamma_1}^{\infty}(\gamma_{\text{th}}) + F_{\tilde{\gamma}_2}^{\infty}(\gamma_{\text{th}}), \end{aligned} \tag{33}$$

where $F_{\gamma_1}^{\infty}(x)$ and $F_{\tilde{\gamma}_2}^{\infty}(x)$ represent the CDF of $\gamma_1$ and $\tilde{\gamma}_2$ in the high SNR region, respectively. Using Eq. (07.34.06.0006.01) in Wolfram (2010), $F_{\gamma_1}^{\infty}(x)$ can be obtained as

$$F_{\gamma_1}^{\infty}(x) = \mu\left(\frac{x}{\bar{\gamma}_1}\right)^{\frac{\beta}{2}} + o\left(\left(\frac{1}{\bar{\gamma}_1}\right)^{\frac{\beta}{2}}\right), \tag{34}$$

where $\mu = \frac{(\alpha\beta)^{\beta}\Gamma(\alpha-\beta)}{\Gamma(\alpha)\Gamma(\beta+1)}$ and $o(\cdot)$ denotes the higher-order infinitesimal of higher order. Using the Maclaurin series of the exponential function and retaining the lowest order term, $F_{\tilde{\gamma}_2}^{\infty}(x)$ can be written as

$$F_{\tilde{\gamma}_2}^{\infty}(x) = \frac{a_1}{\bar{\gamma}_2}x + o\left(\frac{1}{\bar{\gamma}_2}\right). \tag{35}$$

By substituting Eqs. (34) and (35) into Eq. (33), the OP expression in high SNR with diversity order and coding gain can be approximated as (Bankey et al., 2018)

$$P_{\text{out}}^{\infty}(\gamma_{\text{th}}) \approx (G_{\text{c}}\bar{\gamma})^{-G_{\text{d}}}. \tag{36}$$

Thereby, the diversity order $G_{\text{d}}$ and coding gain $G_{\text{c}}$ are, respectively, given by

$$G_{\text{d}} = \min\left(1, \frac{\beta}{2}\right), \tag{37}$$

and

$$G_{\text{c}} = \begin{cases} \frac{\mu^{-\frac{2}{\beta}}}{\gamma_{\text{th}}}, & \frac{\beta}{2} < 1, \\ \frac{1}{a_1\gamma_{\text{th}}}, & \frac{\beta}{2} > 1. \end{cases} \tag{38}$$

## 5 Numerical results

In this section, simulation results are provided to confirm the correctness of theoretical analysis and to further showcase the effects of phase errors

on the outage performance of the considered system. In the simulation, we assume that the FSO feeder link undergoes Gamma-Gamma fading with different channel parameters in terms of weak turbulence ($\alpha = 2.902, \beta = 2.51$), moderate turbulence ($\alpha = 2.296, \beta = 1.822$), and strong turbulence ($\alpha = 2.064, \beta = 1.342$) (Zedini et al., 2015). On the other hand, the mmWave user link subject to SR fading is assumed to have three different channel fading conditions, namely, heavy shadowing (HS) ($b = 0.063, m = 2, \Omega = 0.0007$), and average shadowing (AS) ($b = 0.251, m = 5, \Omega = 0.279$) (Abdi et al., 2003). All plots are conducted with $\bar{\gamma} = \bar{\gamma}_1 = \bar{\gamma}_2$. In addition, other main simulation parameters are listed in Table 1 (Huang XJ et al., 2019; Lin et al., 2019).

**Table 1 Main simulation parameters**

| Parameter | Value |
|---|---|
| Orbit | GEO |
| Carrier frequency, $f$ | 73.5 GHz |
| Maximum beam gain, $G_{\mathrm{t,max}}$ | 52 dBi |
| 3 dB angle, $\theta_{\mathrm{3dB}}$ | 0.4° |
| Noise bandwidth, $B$ | 5 GHz |
| Noise temperature, $T$ | 300 K |

The effects of phase errors on the output SNR of the system are depicted in Fig. 3. The FSO feeder link is subject to weak turbulence, the mmWave user link is subject to SR fading with AS, and the antennas number $N = 16$. It can be seen that the SNR performance decreases as the standard variance of the phase error increases, which is expected according to Eqs. (12) and (18).

Figs. 4 and 5 depict the outage performance of different channel fading for the mmWave user link and FSO feeder link, respectively, in the case when $\gamma_{\mathrm{th}} = 0$ dB, $N = 256$, and $\sigma^2 = 0.6$. Obviously, the analytical results agree well with the Monte Carlo simulations, confirming the validity of the theoretical formulas. Meanwhile, the asymptotic OP curves are consistent with analytical results in the high SNR. In addition, the performance in both Figs. 4 and 5 is greatly reduced when severe fading is present. In particular, Fig. 4 reveals the same diversity order but different coding gain, where the diversity order is 1, which can apparently be shown in Eq. (37).

Fig. 6 shows the OP of two different phase errors of the user link with respect to various numbers of antennas. Here, we assume that the FSO feeder link

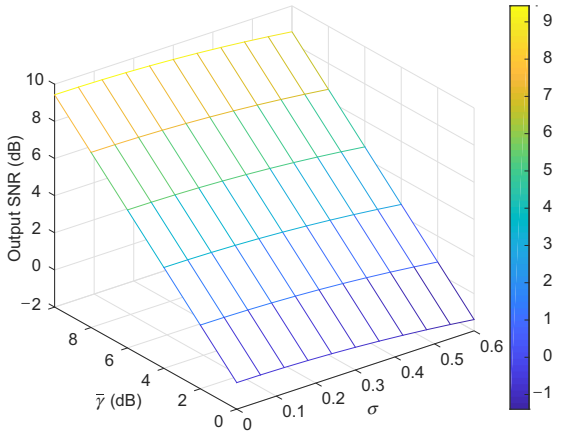


**Fig. 3 Output SNR of the system with different phase errors**

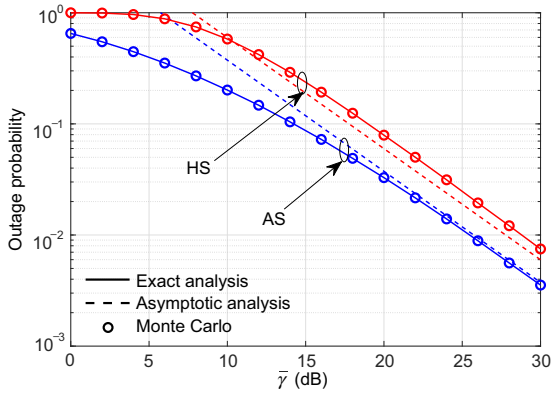


**Fig. 4 Outage probability versus $\bar{\gamma}$ with different SR fading for the user link (HS: heavy shadowing; AS: average shadowing)**

follows weak turbulence and that the mmWave user link follows AS fading while $\gamma_{\mathrm{th}} = 0$ dB. A noteworthy observation is that the outage performance improves as the number of antennas increases or the phase error decreases. In addition, the effect of the phase error on the system performance is more evident when $N = 16$ than when $N = 256$. This is because the antenna gain is great enough to reduce the effect of the phase error when the number of antennas is large.

## 6 Conclusions

In this paper, we have analyzed the outage performance of an aeronautical broadband satellite communication system with the AF protocol. With the help of the location-based BF weight vector, we have derived the exact and asymptotic expressions

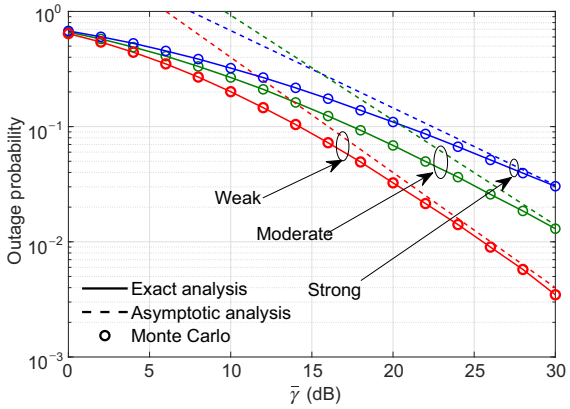


**Fig. 5 Outage probability versus $\bar{\gamma}$ with different Gamma-Gamma fading for the feeder link**

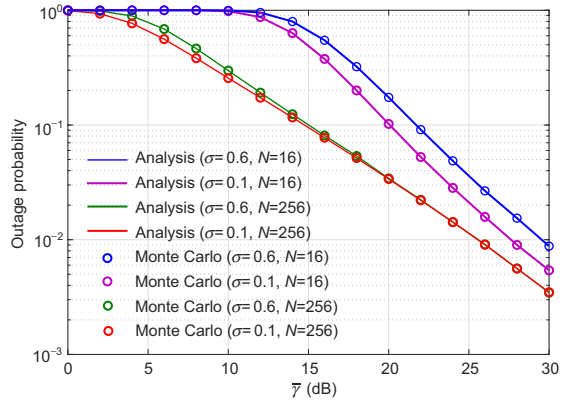


**Fig. 6 Outage probability versus $\bar{\gamma}$ with different antenna numbers and phase errors**

for the OP of the forward link of the considered system, in which the phase error has been taken into account in the user link. Finally, simulation results have shown notable effects of phase errors on the overall system performance. Our findings provide valuable insight into the aeronautical broadband satellite communications.

## Contributors

Min LIN designed the research. Huaicong KONG and Xiaoyu LIU conducted the derivation and validation. Huaicong KONG and Jian OUYANG drafted the manuscript. Shiwen HE and Weiping ZHU helped organize the manuscript. Shiwen HE and Weiping ZHU revised and finalized the paper.

## Compliance with ethics guidelines

Huaicong KONG, Min LIN, Shiwen HE, Xiaoyu LIU, Jian OUYANG, and Weiping ZHU declare that they have no conflict of interest.

## References

Abdi A, Lau WC, Alouini MS, et al., 2003. A new simple model for land mobile satellite channels: first- and second-order statistics. *IEEE Trans Wirel Commun*, 2(3):519-528. https://doi.org/10.1109/TWC.2003.811182

Ahmad I, Nguyen KD, Letzepis N, 2017. Performance analysis of high throughput satellite systems with optical feeder links. Proc IEEE Global Communications Conf, p.1-7. https://doi.org/10.1109/GLOCOM.2017.8255105

Andrews LC, Phillips RL, 2005. Laser Beam Propagation Through Random Media (2nd Ed.). SPIE Press. https://doi.org/10.1117/3.626196

Bankey V, Upadhyay PK, Costa DBD, et al., 2018. Performance analysis of multi-antenna multiuser hybrid satellite-terrestrial relay systems for mobile services delivery. *IEEE Access*, 6:24729-24745. https://doi.org/10.1109/ACCESS.2018.2830801

Chayot R, Thomas N, Poulliat C, et al., 2017. Channel estimation and equalization for CPM with application for aeronautical communications via a satellite link. Proc IEEE Military Communications Conf, p.888-893. https://doi.org/10.1109/MILCOM.2017.8170746

Cianca E, Rossi T, Ruggieri M, et al., 2018. Softwarization and virtualization as enablers for future EHF/FSO high throughput satellites. Proc IEEE Global Communications Conf, p.1-6. https://doi.org/10.1109/GLOCOM.2018.8647698

Gerbracht S, Scheunert C, Jorswieck EA, 2012. Secrecy outage in MISO systems with partial channel information. *IEEE Trans Inform Forens Secur*, 7(2):704-716. https://doi.org/10.1109/TIFS.2011.2181946

Gradshteyn IS, Ryzhik IM, 2007. Table of Integrals, Series and Products (7th Ed.). Academic Press, New York, USA. https://doi.org/10.2307/2007757

Huang QQ, Lin M, Wang JB, et al., 2020a. Energy efficient beamforming schemes for satellite-aerial-terrestrial networks. *IEEE Trans Commun*, 68(6):3863-3875. https://doi.org/10.1109/TCOMM.2020.2978044

Huang QQ, Lin M, Zhu WP, et al., 2020b. Performance analysis of integrated satellite-terrestrial multiantenna relay networks with multiuser scheduling. *IEEE Trans Aerosp Electron Syst*, 56(4):2718-2731. https://doi.org/10.1109/TAES.2019.2952698

Huang XJ, Zhang JA, Liu RP, et al., 2019. Airplane-aided integrated networking for 6G wireless: will it work? *IEEE Veh Technol Mag*, 14(3):84-91. https://doi.org/10.1109/MVT.2019.2921244

Illi E, Bouanani FE, Ayoub F, et al., 2020. A PHY layer security analysis of a hybrid high throughput satellite with an optical feeder link. *IEEE Open J Commun Soc*, 1:713-731. https://doi.org/10.1109/OJCOMS.2020.2995327

Jacob P, Sirigina RP, Madhukumar AS, et al., 2017. Cognitive radio for aeronautical communications: a survey. *IEEE Access*, 4:3417-3443. https://doi.org/10.1109/ACCESS.2016.2570802

Kapusuz KY, Sen Y, Bulut M, et al., 2016. Low-profile scalable phased array antenna at Ku-band for mobile satellite communications. Proc IEEE Int Symp on

Phased Array Systems and Technology, p.1-4. https://doi.org/10.1109/ARRAY.2016.7832648

Kaushal H, Kaddoum G, 2017. Optical communication in space: challenges and mitigation techniques. *IEEE Commun Surv Tut*, 19(1):57-96. https://doi.org/10.1109/COMST.2016.2603518

Kong HC, Lin M, Zhu WP, et al., 2020. Multiuser scheduling for asymmetric FSO/RF links in satellite-UAV-terrestrial networks. *IEEE Wirel Commun Lett*, 9(8):1235-1239. https://doi.org/10.1109/LWC.2020.2986750

Lin Z, Lin M, Ouyang J, et al., 2019. Robust secure beamforming for multibeam satellite communication systems. *IEEE Trans Veh Technol*, 68(6):6202-6206. https://doi.org/10.1109/TVT.2019.2913793

Lin Z, Lin M, Zhu WP, et al., 2020a. Robust secure beamforming for wireless powered cognitive satellite-terrestrial networks. *IEEE Trans Cogn Commun Netw*, online. https://doi.org/10.1109/TCCN.2020.3016096

Lin Z, Lin M, Champagne B, et al., 2020b. Secure beamforming for cognitive satellite terrestrial networks with unknown eavesdroppers. *IEEE Syst J*, online. https://doi.org/10.1109/JSYST.2020.2983309

Lyras NK, Kourogiorgas CI, Kapsis TT, et al., 2019. Ground-to-satellite optical link turbulence effects: propagation modelling & transmit diversity performance. Proc 13th European Conf on Antennas and Propagation, p.1-5.

Mengali A, Kayhan F, Shankar B, et al., 2016. Exploiting diversity in future generation satellite systems with optical feeder links. Proc 34th Int Communications Satellite Systems Conf, p.1-10. https://doi.org/10.2514/6.2016-5768

Morales-Ferre R, Richter P, Falletti E, et al., 2020. A survey on coping with intentional interference in satellite navigation for manned and unmanned aircraft. *IEEE Commun Surv Tut*, 22(1):249-291. https://doi.org/10.1109/COMST.2019.2949178

Mullen K, 1967. The teacher's corner: a note on the ratio of two independent random variables. *Am Stat*, 21(3):30-31. https://doi.org/10.1080/00031305.1967.10479818

Rao JBL, Mital R, Patel DP, et al., 2013. Low-cost multibeam phased array antenna for communications with GEO satellites. *IEEE Aerosp Electron Syst Mag*, 28(6):32-37. https://doi.org/10.1109/MAES.2013.6533742

Sacchi C, Rossi T, Murroni M, et al., 2019. Extremely high frequency (EHF) bands for future broadcast satellite services: opportunities and challenges. *IEEE Trans Broadcast*, 65(3):609-626. https://doi.org/10.1109/TBC.2019.2892655

Trinh PV, Pham AT, 2015. Outage performance of dual-hop AF relaying systems with mixed MMW RF and FSO links. Proc IEEE 82nd Vehicular Technology Conf, p.1-5. https://doi.org/10.1109/VTCFall.2015.7391061

Winters JH, Luddy MJ, 2019. Phased array applications to improve troposcatter communications. Proc IEEE Int Symp on Phased Array System & Technology, p.1-4. https://doi.org/10.1109/PAST43306.2019.9020793

Wolfram I, 2010. Mathematica Edition: Version 80. https://functions.wolfram.com

Zedini E, Ansari IS, Alouini MS, 2015. Performance analysis of mixed Nakagami-$m$ and Gamma-Gamma dual-hop FSO transmission systems. *IEEE Photon J*, 7(1):7900120.

Zedini E, Kammoun A, Alouini MS, 2020. Performance of multibeam very high throughput satellite systems based on FSO feeder links with HPA nonlinearity. *IEEE Trans Wirel Commun*, 19(9):5908-5923. https://doi.org/10.1109/TWC.2020.2998139

Zhang YH, Huang WH, Li P, et al., 2019. Analysis of influence of channel damage on phased array communication links. Proc IEEE-APS Topical Conf on Antennas and Propagation in Wireless Communications, p.306-310. https://doi.org/10.1109/APWC.2019.8870475

## Appendix A: Proof of Lemma 1

Letting $\tau \in [0,1]$, the BF vector $\boldsymbol{w}(\tau)$ that maximizes the expected output SNR in Eq. (3) can be expressed as (Gerbracht et al., 2012)

$$\boldsymbol{w}(\tau) = \sqrt{\tau}\bar{\boldsymbol{w}} + \sqrt{1-\tau}\tilde{\boldsymbol{w}}, \tag{A1}$$

where $\bar{\boldsymbol{w}} = \frac{\boldsymbol{a}(\theta_0)}{\sqrt{N}}$ and $\tilde{\boldsymbol{w}}$ is the orthogonal complement vector of $\bar{\boldsymbol{w}}$. By substituting Eq. (A1) into the expected output SNR in Eq. (3), we have

$$\mathbb{E}[\gamma] = \mathbb{E}\left[\frac{\gamma_1\gamma_2}{\gamma_1+\gamma_2+1}\right] \approx \frac{\mathbb{E}[\gamma_2]\,\Xi}{\mathbb{E}[\gamma_2]+\Xi+1}, \tag{A2}$$

where $\Xi = \mathbb{E}[\gamma_1]$ is a constant and "$\approx$" holds when Mullen's inequality is used (Mullen, 1967). Further, by substituting Eq. (A1) into Eq. (A2), with the help of Eq. (8), $\mathbb{E}[\gamma_2]$ can be expressed as

$$\mathbb{E}[\gamma_2] = \bar{\gamma}_2\mathbb{E}\left[\left|\left(\sqrt{\tau}\bar{\boldsymbol{w}} + \sqrt{1-\tau}\tilde{\boldsymbol{w}}\right)^{\mathrm{H}}(\rho\boldsymbol{a}(\theta_0)+\tilde{\boldsymbol{g}})\right|^2\right]. \tag{A3}$$

According to the orthogonality principle, $\mathbb{E}[\gamma_2]$ in Eq. (A3) can be rewritten as

$$\begin{aligned}\mathbb{E}[\gamma_2] = \bar{\gamma}_2\Big(&\tau\left|\bar{\boldsymbol{w}}^{\mathrm{H}}\boldsymbol{a}(\theta_0)\right|^2\mathbb{E}\left[\rho^2\right] \\ &+\tau\mathbb{E}\left[\left|\bar{\boldsymbol{w}}^{\mathrm{H}}\tilde{\boldsymbol{g}}\right|^2\right] + (1-\tau)\,\mathbb{E}\left[\left|\tilde{\boldsymbol{w}}^{\mathrm{H}}\tilde{\boldsymbol{g}}\right|^2\right]\Big),\end{aligned} \tag{A4}$$

where $\mathbb{E}\left[\rho^2\right] = \Omega$ and $\mathbb{E}\left[\left|\bar{\boldsymbol{w}}^{\mathrm{H}}\tilde{\boldsymbol{g}}\right|^2\right] = \mathbb{E}\left[\left|\tilde{\boldsymbol{w}}^{\mathrm{H}}\tilde{\boldsymbol{g}}\right|^2\right] = 2b$. Therefore, using $\bar{\boldsymbol{w}} = \frac{\boldsymbol{a}(\theta_0)}{\sqrt{N}}$ in Eq. (A4), Eq. (A3) can be finally denoted as

$$\mathbb{E}[\gamma_2] = \bar{\gamma}_2(\tau N\Omega + 2b). \tag{A5}$$

As a matter of fact, one can easily find that only when $\tau = 1$, can the maximum value of $\mathbb{E}[\gamma]$ be obtained.

## Appendix B: Calculation of $\theta_0$

As shown in Fig. 2, we first derive the value of $\cos\theta_{\mathrm{p}}$ with respect to longitude difference $\varphi_{\mathrm{a}}$ and latitude $\theta_{\mathrm{a}}$. In Fig. 2a, the projection of point $B$ on $OA$ can be expressed as $R\cos\varphi_{\mathrm{a}}$ with $R$ being the Earth's radius; the projection of point $C$ on $OB$ can be denoted as $R\cos\theta_{\mathrm{a}}$. Therefore, the projection of point $C$ on $OA$ is given by $R\cos\theta_{\mathrm{a}}\cos\varphi_{\mathrm{a}}$. On another front, the projection of point $C$ on $OA$ can also be represented by $R\cos\theta_{\mathrm{p}}$, and thus $\cos\theta_{\mathrm{p}} = \cos\theta_{\mathrm{a}}\cos\varphi_{\mathrm{a}}$. Next, in Fig. 2b, the lengths of $CD$ and $SD$ can be, respectively, derived as

$$CD = (R+H)\cos\theta_{\mathrm{p}} - R, \tag{B1}$$

and

$$SD = (R+H)\sin\theta_{\mathrm{p}}, \tag{B2}$$

where $H$ is the height of the GEO satellite. Accordingly, we can obtain

$$\tan\theta_0 = \frac{CD}{SD} = \frac{(R+H)\cos\theta_{\mathrm{p}} - R}{(R+H)\sin\theta_{\mathrm{p}}}, \tag{B3}$$

with $\cos\theta_{\mathrm{p}} = \cos\theta_{\mathrm{a}}\cos\varphi_{\mathrm{a}}$. Then, using $\sin^2\theta_{\mathrm{p}} + \cos^2\theta_{\mathrm{p}} = 1$ and substituting $H = 35\ 786$ km and $R = 6371$ km into Eq. (B3), the expression of $\theta_0$ in Eq. (11) can be easily derived.

## Appendix C: Proof of Lemma 2

In the phased array antenna, the actual phase shift of the $n^{\mathrm{th}}$ antenna element can be denoted as $\tilde{\theta}_0 = \theta_0 + \varepsilon_n$, where $\tilde{\theta}_0$ is the ideal phase shift in $\boldsymbol{a}(\theta_0)$ and $\varepsilon_n$ is the random phase error. Hence, the actual receive BF vector $\boldsymbol{v}$ can be expressed as

$$\boldsymbol{v} = \mathrm{e}^{\mathrm{j}\boldsymbol{\Lambda}}\boldsymbol{w}^*, \tag{C1}$$

where $\boldsymbol{\Lambda} = \mathrm{diag}(\varepsilon_1, \varepsilon_2, \cdots, \varepsilon_N)$. Therefore, the output SNR of the user link can be rewritten as

$$\tilde{\gamma}_2 = \bar{\gamma}_2\left|\boldsymbol{v}^{\mathrm{H}}\boldsymbol{g}\right|^2. \tag{C2}$$

To facilitate the analysis of the impact of phase disturbance on the output SNR of the user link, we use the Taylor series to further expand the actual phase complex number. The Taylor series expansion is given by (Gradshteyn and Ryzhik, 2007)

$$\mathrm{e}^{\mathrm{j}x} = \sum_{i=0}^{\infty}\mathrm{e}^{\mathrm{j}x_0}\frac{(\mathrm{j}\Delta x)^i}{i!} \approx \mathrm{e}^{\mathrm{j}x_0}\left(1 + \mathrm{j}\Delta x - \frac{\Delta x^2}{2!}\right). \tag{C3}$$

The approximation is valid when the relationship is sufficiently small.

On the other hand, $\left|\boldsymbol{v}^{\mathrm{H}}\boldsymbol{a}(\theta_0)\right|^2$ can be expressed as

$$\begin{aligned}\left|\boldsymbol{v}^{\mathrm{H}}\boldsymbol{a}(\theta_0)\right|^2 &= \left|(\boldsymbol{w}^*)^{\mathrm{H}}\mathrm{e}^{-\mathrm{j}\boldsymbol{\Lambda}}\boldsymbol{a}(\theta_0)\right|^2 \\ &= \left|\sum_{n=1}^{N} w_n a_n(\theta_0)\,\mathrm{e}^{-\mathrm{j}\varepsilon_n}\right|^2 \triangleq \left|\sum_{n=1}^{N}\mathrm{e}^{\mathrm{j}\varphi_n}\mathrm{e}^{-\mathrm{j}\varepsilon_n}\right|^2,\end{aligned} \tag{C4}$$

where $w_n$ and $a_n(\theta_0)$ are the corresponding elements of the BF weight vector $\boldsymbol{w}^*$ and the array steering vector $\boldsymbol{a}(\theta_0)$, respectively. In addition, $\varphi_n$ is the phase of $w_n a_n(\theta_0)$, i.e., $w_n a_n(\theta_0) = \mathrm{e}^{\mathrm{j}\varphi_n}$. According to the Taylor series expansion Eq. (C3), along with the Euler formula (Gradshteyn and Ryzhik, 2007), we can further expand Eq. (C4) as

$$\begin{aligned}&\left|\boldsymbol{v}^{\mathrm{H}}\boldsymbol{a}(\theta_0)\right|^2 \\ &= \left|\sum_{n=1}^{N}\mathrm{e}^{\mathrm{j}\varphi_n}\left(1 - \mathrm{j}\varepsilon_n - \frac{\varepsilon_n^2}{2}\right)\right|^2 \\ &= \underbrace{\left[\sum_{n=1}^{N}\left(1-\frac{\varepsilon_n^2}{2}\right)\cos\varphi_n + \sum_{n=1}^{N}\varepsilon_n\sin\varphi_n\right]^2}_{\Psi_1} \\ &\quad + \underbrace{\left[\sum_{n=1}^{N}\left(1-\frac{\varepsilon_n^2}{2}\right)\sin\varphi_n - \sum_{n=1}^{N}\varepsilon_n\cos\varphi_n\right]^2}_{\Psi_2}.\end{aligned} \tag{C5}$$

Applying Eqs. (13)–(17), the expectations of $\Psi_1$ and $\Psi_2$ in Eq. (C5) are, respectively, given by Eqs. (C6) and (C7) (at the top of the next page).

By summing up Eqs. (C6) and (C7), we can obtain Eq. (C8) (at the top of the next page). By substituting Eq. (10) into Eq. (C8), the expectation of $\left|\boldsymbol{v}^{\mathrm{H}}\boldsymbol{a}(\theta_0)\right|^2$ can be denoted as

$$\mathbb{E}\left[\left|\boldsymbol{v}^{\mathrm{H}}\boldsymbol{a}(\theta_0)\right|^2\right] = N + \sigma^2 - N\sigma^2. \tag{C9}$$

Towards this, the output SNR of the user link can be expressed as Eq. (18).

By denoting $\tilde{\boldsymbol{g}} = [g_1, g_2, \cdots, g_N]$ and $\boldsymbol{v} = [v_1, v_2, \cdots, v_N] = \left[|v_1|\,\mathrm{e}^{\mathrm{j}\xi_1}, |v_2|\,\mathrm{e}^{\mathrm{j}\xi_2}, \cdots, |v_N|\,\mathrm{e}^{\mathrm{j}\xi_N}\right]$, we can obtain

$$\boldsymbol{v}^{\mathrm{H}}\tilde{\boldsymbol{g}} = \sum_{n=1}^{N}|v_n|g_n\mathrm{e}^{\mathrm{j}\xi_n}. \tag{C10}$$

$$\mathbb{E}[\Psi_1]=\mathbb{E}\left\{\left[\sum_{n=1}^{N}\left(1-\frac{\varepsilon_n^2}{2}\right)\cos\varphi_n+\sum_{n=1}^{N}\varepsilon_n\sin\varphi_n\right]^2\right\}=\left(\sum_{n=1}^{N}\cos\varphi_n\right)^2-\sigma^2\left(\sum_{n=1}^{N}\cos\varphi_n\right)^2+\mathbb{E}\left[\left(\sum_{n=1}^{N}\varepsilon_n\sin\varphi_n\right)^2\right]. \tag{C6}$$

$$\mathbb{E}[\Psi_2]=\mathbb{E}\left\{\left[\sum_{n=1}^{N}\left(1-\frac{\varepsilon_n^2}{2}\right)\sin\varphi_n-\sum_{n=1}^{N}\varepsilon_n\cos\varphi_n\right]^2\right\}=\left(\sum_{n=1}^{N}\sin\varphi_n\right)^2-\sigma^2\left(\sum_{n=1}^{N}\sin\varphi_n\right)^2+\mathbb{E}\left[\left(\sum_{n=1}^{N}\varepsilon_n\cos\varphi_n\right)^2\right]. \tag{C7}$$

$$\begin{aligned}\mathbb{E}\left[\left|\boldsymbol{v}^{\mathrm{H}}\boldsymbol{a}\left(\theta_0\right)\right|^2\right]&=\mathbb{E}[\Psi_1]+\mathbb{E}[\Psi_2]\\&=\left(\sum_{n=1}^{N}\cos\varphi_n\right)^2+\left(\sum_{n=1}^{N}\sin\varphi_n\right)^2+\sigma^2-\sigma^2\left[\left(\sum_{n=1}^{N}\cos\varphi_n\right)^2+\left(\sum_{n=1}^{N}\sin\varphi_n\right)^2\right]\\&=\left|\left(\boldsymbol{w}^*\right)^{\mathrm{H}}\boldsymbol{a}\left(\theta_0\right)\right|^2+\sigma^2-\sigma^2\left|\left(\boldsymbol{w}^*\right)^{\mathrm{H}}\boldsymbol{a}\left(\theta_0\right)\right|^2.\end{aligned} \tag{C8}$$

According to $\tilde{\boldsymbol{g}}\sim\mathbb{CN}(0,2b\boldsymbol{I}_N)$, we have that $g_n\sim\mathbb{CN}(0,2b)$ is a complex Gaussian RV. Consequently, $g_n\mathrm{e}^{\mathrm{j}\xi_n}$ in Eq. (C10) can be written as

$$g_n\mathrm{e}^{\mathrm{j}\xi_n}=X_n+\mathrm{j}Y_n, \tag{C11}$$

where $X_n,Y_n\sim\mathbb{N}(0,b)$, thereby resulting in $\sum_{n=1}^{N}|v_n|X_n$, $\sum_{n=1}^{N}|v_n|Y_n\sim\mathbb{N}\left(0,b\|\boldsymbol{v}\|^2\right)$. Using Eqs. (C10) and (C11), we have $\boldsymbol{v}^{\mathrm{H}}\tilde{\boldsymbol{g}}=\sum_{n=1}^{N}|v_n|X_n+\mathrm{j}\sum_{n=1}^{N}|v_n|Y_n$, which is a complex Gaussian RV with average power $2b\|\boldsymbol{v}\|^2$. As for the first term of Eq. (18), we can find that $\rho\sqrt{\Phi}$ is a Nakagami-$m$ RV with average power $\Phi\Omega$ and severity parameter $m$. In a manner similar to Huang QQ et al. (2020a), the PDF of $\tilde{\gamma}_2=\bar{\gamma}_2\left(\left|\rho\sqrt{\Phi}+\boldsymbol{v}^{\mathrm{H}}\tilde{\boldsymbol{g}}\right|^2\right)$ can be obtained as

$$f_{\tilde{\gamma}_2}(x)=\frac{a_1}{\bar{\gamma}_2}\exp\left(-\frac{a_2x}{\bar{\gamma}_2}\right){}_1F_1\left(m,1,\frac{a_3x}{\bar{\gamma}_2}\right), \tag{C12}$$

where $a_1$, $a_2$, and $a_3$ are as given in Lemma 2. In this study, we consider a reasonable assumption of $m\in\mathbb{N}^+$. As a result, the PDF of $\tilde{\gamma}_2$ in terms of $m\in\mathbb{N}^+$ can be expressed as a finite series expansion, namely (Huang QQ et al., 2020a)

$$\begin{aligned}f_{\tilde{\gamma}_2}(x)=&a_1\exp\left(-\frac{(a_2-a_3)x}{\bar{\gamma}_2}\right)\\&\cdot\sum_{k=0}^{m-1}\frac{(1-m)_k(-a_3)^k}{\bar{\gamma}_2^{k+1}(k!)^2}x^k.\end{aligned} \tag{C13}$$

With the help of Eqs. (3.351.1) and (3.351.3) in Gradshteyn and Ryzhik (2007), the CDF of $\tilde{\gamma}_2$ can be expressed as Eq. (19) in Lemma 2.